# Studies of Synthetic Peptides of Human Apolipoprotein A-I Containing Tandem Amphipathic α-Helixes†

Vinod K. Mishra,‡ Mayakonda N. Palgunachari,‡ Geeta Datta,‡ Michael C. Phillips,§ Sissel Lund-Katz,§ Samuel O. Adeyeye, Jere P. Segrest,‡ and G. M. Anantharamaiah*,‡

*Departments of Medicine, Biochemistry and Molecular Genetics, and the Atherosclerosis Research Unit D640, 1808 Seventh Avenue South, UAB Medical Center, Birmingham, Alabama 35294, and The Department of Biochemistry, Allegheny University of The Health Sciences, Philadelphia, Pennsylvania 19129*

*Received January 7, 1998; Revised Manuscript Received April 20, 1998*

ABSTRACT: In mature human apolipoprotein A-I (apo A-I), the amino acid residues 1−43 are encoded by exon 3, whereas residues 44−243 are encoded by exon 4 of the apo A-I gene. The region encoded by exon 4 of the apo A-I gene contains 10 tandem amphipathic α-helixes; their location and the class to which they belong are as follows: helix 1 (44−65, class $A_1$), helix 2 (66−87, class $A_1$), helix 3 (88−98, class Y), helix 4 (99−120, class Y), helix 5 (121−142, class $A_1$), helix 6 (143−164, class $A_1$), helix 7 (165−186, class $A_1$), helix 8 (187−208, class $A_1$), helix 9 (209−219, class Y), and helix 10 (220−241, class Y). To examine the effects of multiple tandem amphipathic helixes compared to individual helixes of apo A-I on lipid association, we have studied lipid-associating properties of the following peptides: Ac-44−87-$NH_2$ (peptide 1−2), Ac-66−98-$NH_2$ (peptide 2−3), Ac-66−120-$NH_2$ (peptide 2−3−4), Ac-88−120-$NH_2$ (peptide 3−4), Ac-99−142-$NH_2$ (peptide 4−5), Ac-121−164-$NH_2$ (peptide 5−6), Ac-143−186-$NH_2$ (peptide 6−7), Ac-165−208-$NH_2$ (peptide 7−8), Ac-187−219-$NH_2$ (peptide 8−9), and Ac-209−241-$NH_2$ (peptide 9−10). To study lipid-associating properties of the region encoded by exon 3 of the apo A-I gene, 1−33-$NH_2$ (peptide G*) has also been studied. The results of the present study indicate that, among the peptides studied, peptides 1−2 and 9−10 possess significantly higher lipid affinity than the other peptides, with peptide 9−10 having higher lipid affinity than peptide 1−2, as evidenced by (i) higher helical content in the presence of 1,2-dimyristoyl-*sn*-glycero-3-phosphocholine (DMPC), (ii) faster rate of association with DMPC multilamellar vesicles (MLV), (iii) greater reduction in the enthalpy of gel to liquid−crystalline phase transition of DMPC MLV, (iv) higher exclusion pressure from an egg yolk phosphatidylcholine monolayer, and (v) higher partitioning into 1-palmitoyl-2-oleoyl-*sn*-glycero-3-phosphocholine MLV. A comparison of the free energies of lipid association ($\Delta G$) of the peptides studied here with those studied previously by us [Palgunachari, M. N., et al. (1996) *Arterioscler. Thromb. Vasc. Biol. 16*, 328−338] indicates that, except for the peptides 4−5 and 5−6, other peptides possess higher lipid affinities compared to constituent helixes. However, the lipid affinities of the peptides studied here are neither higher than nor equal to the sum of the lipid affinities of the constituent helixes. This indicates the absence of cooperativity among the adjacent amphipathic helical domains of apo A-I for lipid association. As indicated by $\Delta G$, the lipid affinity of peptide 4−5 is higher than peptide 5 but lower than peptide 4; the lipid affinity of peptide 5−6 is lower than both peptides 5 and 6. Implications of these results for the structure and function of apo A-I are discussed.

Human apolipoprotein A-I (apo A-I)[1] is the major protein component of high-density lipoproteins (HDL) and has been shown to regress atherosclerosis in transgenic animals (*1*−*3*). That the HDL particle containing apo A-I alone is exclusively involved in the protective effect (*4*) provides compelling evidence for the antiatherogenicity of human apo A-I. The structural motif responsible for the lipid interaction in apo A-I has been postulated to be the amphipathic α-helix and several lines of experimental evidence provide strong support for this hypothesis (*5*, *6*). This protein is also involved in the activation of the plasma enzyme lecithin: cholesterol acyltransferase (LCAT) (*7*) and in mediating efflux of cellular cholesterol (*8*−*10*).

† This research is supported by NIH Program Project Grants HL34343 and HL22633.

* To whom correspondence should be addressed. Tel: (205) 934-1884. Fax: (205) 975-8079. E-mail: ananth@uab.edu.

‡ UAB Medical Center.

§ Allegheny University of the Health Sciences.

[1] Abbreviations: Ac, acetyl; apo A-I, human apolipoprotein A-I; CD, circular dichroism; DCC, dicyclohexylcarbodiimide; DMPC, 1,2-dimyristoyl-*sn*-glycero-3-phosphocholine; DSC, differential scanning calorimetry; EM, electron microscopy; EYPC, egg yolk phosphatidylcholine; Fmoc, 9-fluorenylmethoxycarbonyl; Gdn·HCl, guanidinium hydrochloride; HDL, high-density lipoproteins; HOBT, 1-hydroxybenzotriazole; $K_p$, partition coefficient; LCAT, lecithin:cholesterol acyltransferase; MLV, multilamellar vesicles; $NH_2$, amide; PBS, phosphate-buffered saline; PITC, phenyl isothiocyanate; PPC, 1-palmitoyl-2-hydroxy-*sn*-glycero-3-phosphocholine; POPC, 1-palmitoyl-2-oleoyl-*sn*-glycero-3-phosphocholine; RP-HPLC, reversed-phase high-performance liquid chromatography.

S0006-2960(98)00042-7 CCC: $15.00 
Published on Web 06/25/1998

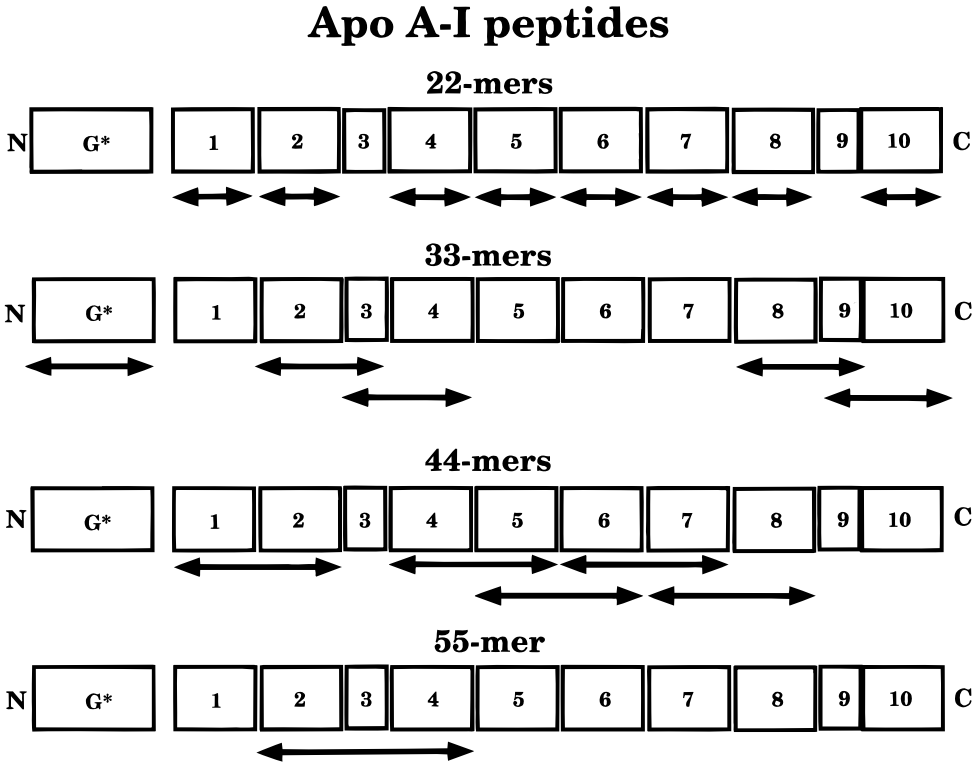


FIGURE 1: Schematic representation of human apo A-I structure indicating the location of 22mer and 11mer (1−10) amphipathic helical segments encoded by exon 4 of the apo A-I gene. Location of the G* helix (*23*) in the region encoded by exon 3 of the apo A-I gene is also indicated. Double-headed arrows indicate apo A-I peptides studied in the present work (33mers, 44mers, and 55mer). The 22mers studied previously by us (*16*) are also indicated. The residue numbers in 22mer and 11mer helixes and the class to which each amphipathic helix belongs to are as follows (*23, 55*): 44−65 (1, class $A_1$), 66−87 (2, class $A_1$), 88−98 (3, class Y), 99−120 (4, Class Y), 121−142 (5, class $A_1$), 143−164 (6, class $A_1$), 165−186 (7, class $A_1$), 187−208 (8, class $A_1$), 209−219 (9, class Y), and 220−241 (10, class Y).

There are eight 22mer and two 11mer putative amphipathic helical domains in the region encoded by exon 4 of the apo A-I gene (Figure 1). These domains are as follows: 1, 44−65; 2, 66−87; 3, 88−98; 4, 99−120; 5, 121−142; 6, 143−164; 7, 165−186; 8, 187−208; 9, 209−219; and 10, 220−241. There is compelling evidence in the literature to suggest that most of the amphipathic helical domains in the apo A-I molecule are lipid associated (*11*−*14*). Apo A-I in the reconstituted lipoprotein particles is more refractory to denaturing agents than free apo A-I, indicating the increased stability of amphipathic helical segments in lipid-associated apo A-I (*15*). As suggested by many investigators, the overall structural organization of apo A-I in discoidal and spherical lipoprotein particles indicates the existence of stabilizing interactions between adjacent amphipathic helical domains (*6*). Recently, our studies of the eight 22mer amphipathic helical domains of human apo A-I have shown that the two end terminal 22mer helixes possess significantly higher lipid affinity than the other helixes (*16*). In the present study, we ask the question whether cooperativity among the adjacent amphipathic helixes plays a major role in determining the lipid-associating properties of the apo A-I molecule.

The lipid-associating properties of apo A-I peptides containing α-helical domains have been studied previously by other investigators (*17*). It was observed that, among the two peptides, apo A-I (158−168) and apo A-I (147−168), only the longer peptide associated with phospholipid (*18*). Fukushima et al. (*19*) synthesized apo A-I (144−165) and apo A-I (121−164) and found that cooperativity is not a major factor in the surface affinity of apo A-I fragments. The peptides apo A-I (165−185), apo A-I(195−243), apo A-I(202−243), and apo A-I(218−243) associated with phospholipid, whereas the peptide apo A-I (225−243) did not (*20*). A 39 residue peptide corresponding to the region 145−183 was studied by Vanloo et al. (*21*). On the basis of the results of their studies, the authors suggested stable peptide−lipid complex formation facilitated by the cooperativity between pairs of helixes (*21*). Thus, although the existence of cooperativity among adjacent amphipathic α-helixes in apo A-I for lipid association has been suggested previously, no systematic studies are as yet available to address this issue for the entire amphipathic helical region of the apo A-I molecule. Toward this, we have studied the lipid-associating properties of five 33mer, five 44mer, and a 55mer peptide encompassing the entire region encoded by exons 3 and 4 of the apo A-I gene.

There are five adjacent 22mer dimer combinations and four adjacent 22mer and 11mer or 11mer and 22mer combinations possible in the apo A-I sequence encoded by exon 4 of the apo A-I gene (Figure 1). The 44mers that would form tandem dimers are helixes 1−2, 4−5, 5−6, 6−7, and 7−8. The 33mers that would form tandem dimers of an 11mer and a 22mer or a 22mer and an 11mer are helixes 2−3, 3−4, 8−9, and 9−10. These peptides were synthesized as Ac-peptide-$NH_2$ to facilitate helix stabilization (*22*). To complete the screening of the entire human apo A-I sequence for lipid-associating properties using synthetic peptides, the N-terminal 1−33-$NH_2$ (peptide G*) was also synthesized (Figure 1). This peptide contains the only class G* helix present in apo A-I (*23*) and is encoded by exon 3 of the apo A-I gene. To determine if a 22mer-11mer-22mer combination is superior to the tandem dimers in the 44mers and the

33mers for lipid association, the 55mer, peptide 2−3−4 was also synthesized. The peptides were studied for their interaction with phospholipids using circular dichroism (CD) spectroscopy, right-angle light scattering measurements, negative stain transmission electron microscopy (EM), differential scanning calorimetry (DSC), monolayer exclusion pressure measurements, and partitioning into 1-palmitoyl-2-oleoyl-*sn*-glycero-3-phosphocholine (POPC) multilamellar vesicles (MLV). The lipid affinities of these peptides have been compared with the lipid affinities of the 22mer peptides studied previously by us (*16*).

## MATERIALS AND METHODS

*Materials.* DMPC, POPC, egg yolk phosphatidylcholine (EYPC), and 1-palmitoyl-2-hydroxy-s*n*-glycero-3-phosphocholine (PPC) were purchased from Avanti Polar Lipids, Inc. (Alabaster, AL) and used without further purification. (1S)-(+)-10-camphorsulfonic acid (99%) and guanidinium hydrochloride (Gdn·HCl, 99%) were obtained from Aldrich Chemical Co. (Milwaukee, WI). Triton X-100 was obtained from Fisher Scientific Co. (Orangeburg, NY). All other chemicals used were of highest purity available commercially.

Human apo A-I was isolated from HDL and purified according to the procedures described elsewhere (*24*).

*Peptide Synthesis and Purification.* The peptides were synthesized using an automated solid-phase peptide synthesizer (Advanced ChemTech. Louisville, KY) on a benzhydrylamine resin (cross-linked with 1% divinylbenzene, 0.536 mequiv/g; Peninsula Laboratories, Inc.) support using Fmoc (9-fluorenylmethoxycarbonyl) amino acids in the presence of dicyclohexylcarbodiimide (DCC) and 1-hydroxybenzotriazole (HOBT), as described earlier (*16*). After cleaving the peptide from the solid support, it was extracted with 6 M Gdn·HCl (10 mL × 3/g of peptide resin), dialyzed against water (1000 MW cutoff dialysis tube; Spectrum, Houston, TX), and lyophilized. The peptides were purified using preparative C-4 reversed-phase HPLC (RP-HPLC) column (VYDAC, 22 mm × 25 cm, particle size 10 $\mu$m) on a Beckman HPLC system using a gradient of 10% acetonitrile to 80% acetonitrile (containing 0.1% trifluoroacetic acid, v/v) in 66 min with a flow rate of 4.8 mL/min. The purity of the peptide was checked using analytical RP-HPLC on a Beckman HPLC (System Gold 166) using C-18 column (VYDAC, 4.6 mm × 25 cm, particle size 5 $\mu$m) and a linear gradient of 10 to 70% acetonitrile/water, containing 0.1% TFA, in 60 min.

The purity and authenticity of synthetic peptides were confirmed by subjecting them to amino acid analysis using the PITC method (*25*) and mass spectral analysis using a PE-Sciox APT-III triple quadrupole ion spray mass spectrometer (Toronto, Ontario, Canada).

*Preparation of Peptide Solutions.* Peptides were dissolved in 6 M Gdn·HCl. The peptide solutions were extensively dialyzed (1000 MW cutoff dialysis tube; Spectrum, Houston, TX) against phosphate buffered saline (PBS; $KH_2PO_4$, 1.47 mM; $Na_2HPO_4 \cdot 7H_2O$, 6.45 mM; NaCl, 136.89 mM; KCl, 2.68 mM; pH 7.4). The concentration of peptide in solution was determined in 6 M Gdn·HCl by measuring the absorbance either at 280 nm (for Trp, $\epsilon_{280} = 5500\ M^{-1}\ cm^{-1}$) or at 275 nm (for Tyr $\epsilon_{275} = 1800\ M^{-1}\ cm^{-1}$). For the peptides which neither have Trp nor Tyr, quantitative amino acid analysis was used to determine their concentration in solution.

*Preparation of DMPC Vesicles.* Multilamellar vesicles of DMPC were prepared as follows. About 20 mg of lipid was dissolved in 200 $\mu$L of chloroform in a test tube. The organic solvent was removed by blowing nitrogen gas over it. The residual solvent was removed by storing the test tube under high vacuum at room temperature for 3 h. The thin film of the lipid deposited on the walls of the test tube was hydrated by 10 freeze−thaw cycles (−70 °C, hot water), with vigorous vortexing between each cycle. Lipid concentration was determined using an ashing procedure for total phosphate determination (*26*).

*Circular Dichroism Spectroscopy.* The CD spectra were recorded using an AVIV 62DS spectropolarimeter (Lakewood, NJ) equipped with a thermoelectric temperature controller and interfaced to a personal computer. The instrument was calibrated with (1S)-(+)-10-camphorsulfonic acid (*27*−*29*). The CD spectra were measured from 260 to 190 nm every 0.5 nm with 1 s averaging per point and a 2 nm bandwidth. A 0.01 cm path length cell was used for obtaining the spectra. A few spectra were recorded from 260 to 195 nm using 0.2 cm path length cell. The CD spectra were signal averaged by adding four scans, baseline corrected, and smoothed. All the CD spectra were recorded at 25 °C. Peptide concentrations of 100 $\mu$M or less were used for obtaining CD spectra. Peptide−DMPC complexes for CD studies were prepared by the cholate dialysis procedure (*30*).

The mean residue ellipticity, $[\Theta]_{MRE}$ (deg cm$^2$ dmol$^{-1}$), was calculated using the following equation:

$$[\Theta]_{MRE} = (MRW \times \Theta)/(10cl)$$

where, MRW is the mean residue weight (molecular weight of the peptide divided by the number of amino acids in the peptide), $\Theta$ is the observed ellipticity in degrees, $c$ is the concentration of the peptide in grams per milliliter, and $l$ is the path length of the cell in centimeters. The percent helicity of the peptide was estimated from the following equation:

$$\%\ \alpha\text{-helix} = ([\Theta]_{222} + 3000)/(36\,000 + 3000) \times 100$$

where, $[\Theta]_{222}$ is the mean residue ellipticity at 222 nm (*31*).

*Right-Angle Light-Scattering Measurements.* Association of the peptides and apo A-I with MLV of DMPC was determined by right-angle light-scattering measurements. Peptides and apo A-I were mixed with MLV of DMPC in a 1:1 (w/w) and 1:2 (w/w) ratio, respectively, and the turbidity clarification was followed by measuring the scattered light intensity using an SLM 8100 photon-counting spectrofluorimeter (SLM Instruments, Inc., Urbana, IL) with both excitation and emission monochromators set at 400 nm. The excitation and emission band-passes were 4 nm each. Data were recorded using slow time-based acquisition. All measurements were carried out at 25 °C.

*Electron Microscopy.* The peptide−DMPC and apo A-I−DMPC (lipid to peptide and lipid-to-protein ratio 2:1, w/w) mixtures were subjected to transmission electron microscopy. The mixtures were negatively stained with 2% potassium

phosphotungstate, pH 7.4, and were examined using a Hitachi H7000 electron microscope on carbon-coated Formvar grids.

*Differential Scanning Calorimetry.* High-sensitivity DSC studies were performed using a Microcal MC-2 scanning calorimeter (MicroCal, Inc., Amherst, MA) at a scan rate of 20 °C $h^{-1}$. The lipid multilamellar vesicles and the peptide−lipid mixtures for DSC were prepared as follows. DMPC (approximately 2 mg) was dissolved in chloroform in a test tube and dried by the slow evaporation of chloroform under a stream of dry nitrogen. The residual solvent was removed by keeping the test tube under high vacuum overnight at room temperature. Either buffer alone or buffer containing the peptide was added to the dry lipid film to obtain a lipid/peptide molar ratio of 20:1, and the mixture was incubated overnight at room temperature. Four consecutive scans, with 60 min equilibration time between each scan, were run for the same sample. No significant changes were observed between the first and the last scan. The thermograms were analyzed using software (DA2, Version 2.1) provided by MicroCal., Inc. (Amherst, MA).

*Association of Peptides with POPC MLV.* Association of peptides with MLV of POPC was determined using an ultracentrifugation method (*32*). Briefly, increasing amounts of peptide (5−30 $\mu$M) were added to a constant amount of POPC MLV (8.4 mM). The mixtures were frozen in liquid nitrogen (−70 °C) and thawed in hot water (60 °C) six times, with vortexing between the freeze−thaw cycles, to equilibrate the mixture. The mixture was centrifuged in a tabletop centrifuge (Beckman, model TL100) at 85 K rpm, 4 °C, for 2 h. The amount of free peptide was estimated in the supernatant either by measuring absorbance at 280 or 275 nm or by quantitative amino acid analysis. The partition coefficients and the free energy of association were calculated as described by us earlier (*32, 33*).

*Interaction of Peptides with Phospholipid Monolayers.* The relative affinities of the peptides for the lipid−water interface were determined using a surface balance technique (*34, 35*). An insoluble monolayer of EYPC was spread at the air−water interface (85 $cm^2$) in a circular Teflon dish containing 80 mL of PBS (pH 7.0) at room temperature. The surface pressure ($\pi$) was monitored by the Wilhelmy plate technique using a mica plate connected to a Cahn RTL recording electrobalance. Sufficient EYPC was spread from a 9:1 (v/v) hexane/ethanol solution to give an initial surface pressure ($\pi_i$) in the range 5−35 dyn/cm. Peptides dissolved in PBS (with 1.5 M Gdn·HCl, to ensure a random-coil monomeric state of the peptides) were injected into the subphase to give an initial concentration of 50 $\mu$g/dL. A small Teflon tube, which projected downward through the monolayer into the aqueous subphase, was used for this injection so that the EYPC monolayer was not disrupted. The peptide molecules renatured in the subphase as Gdn·HCl was diluted to a final concentration of ≤1 mM. The solution was stirred continuously with a magnetic stirrer, and the increase in surface pressure ($\Delta\pi_i$) was recorded until a steady-state value was obtained. Steady-state values for $\Delta\pi_i$ were plotted as a function of $\pi_i$. Linear extrapolation of the $\pi_i$ versus $\Delta\pi_i$ curve to $\Delta\pi_i = 0$ dyn/cm gave the exclusion pressure, i.e., the value of $\pi_i$ at which the peptides were no longer able to penetrate the EYPC monolayer.

Table 1: Mass Spectral Analysis of Synthetic Human Apo A-I Peptides

| peptides | average mass from three estimates, Da | standard deviation, (±) | theoretical mass, Da |
|---|---|---|---|
| 11mers | | | |
| peptide 3 | 1326.72 | 0.00 | 1327.54 |
| peptide 9 | 1264.69 | 0.01 | 1265.47 |
| 33mers | | | |
| peptide G* | 3824.75 | 1.15 | 3823.81 |
| peptide 2-3 | 3974.16 | 0.01 | 3974.41 |
| peptide 3-4 | 4211.28 | 0.99 | 4212.79 |
| peptide 8-9 | 3701.76 | 0.50 | 3702.00 |
| peptide 9-10 | 3790.56 | 0.71 | 3790.41 |
| 44mers | | | |
| peptide 1-2 | 5238.35 | 0.71 | 5239.83 |
| peptide 4-5 | 5498.48 | 0.58 | 5500.02 |
| peptide 5-6 | 5112.43 | 2.33 | 5111.80 |
| peptide 6-7 | 5023.32 | 1.35 | 5024.67 |
| peptide 7-8 | 4963.54 | 1.47 | 4964.57 |
| 55mer | | | |
| peptide 2-3-4 | 6860.89 | 1.83 | 6859.6 |

## RESULTS

*Peptide Synthesis and Reversed-Phase HPLC (RP-HPLC).* The peptides synthesized for the present studies are summarized in Figure 1. While RP-HPLC profile of most of the peptides showed one major peak after cleavage from the resin, the peptides containing a methionine residue showed two peaks. Since our earlier observations with synthetic peptides and apo A-I and apo A-II have indicated that the peak with longer retention time is the peak corresponding to the unoxidized methionine (*36, 16*), we isolated this peak and confirmed the identity of the required peptide by amino acid analysis and mass spectral analysis (Table 1). The other major peak was confirmed by mass spectral analysis to contain methionine sulfoxide.

The purity of the peptides as estimated from analytical RP-HPLC was ≥90% (chromatograms not shown). Retention times of 33mer peptides on analytical RP-HPLC column were peptide G*, 32.00 min, peptide 2−3, 36.92 min; peptide 3−4, 29.04 min; peptide 8−9, 23.77 min; and peptide 9−10, 48.40 min. Under identical conditions, retention times of 44mer peptides were peptide 1−2, 41.26 min; peptide 4−5, 30.97 min; peptide 5−6, 27.02 min; peptide 6−7, 25.99 min; and peptide 7−8, 24.09 min. It is noteworthy that among 33mers, peptide 9−10, and among 44mers, peptide 1−2, have the longest retention times. Retention time of the 55mer, peptide 2−3−4, is similar to that of peptide 1−2 (41.69 and 41.26 min, respectively). The retention time of apo A-I under identical conditions is 43.54 min.

*Circular Dichroism Studies.* Secondary structures of the peptides in different environments were determined by CD spectroscopy. The CD spectra of 33mer and 44mer peptides are shown in Figures 2 and 3, respectively. CD spectra of the peptides G*, 1−2, 2−3−4, 3−4, and 9−10, in the presence of DMPC are shown in Figure 4. CD spectra of other peptides in the presence of DMPC could not be obtained because the peptide−DMPC complexes, prepared using the cholate dialysis procedure (*30*), were not optically clear at the end of the dialysis. We chose to use PPC micelles as a mimic of membrane environment because of the identity of its headgroup with that of diacyl phosphatidylcholines present in biological membranes. PPC has been used previously by us (*16*), as well as by others (*37*), as a membrane-mimetic medium.

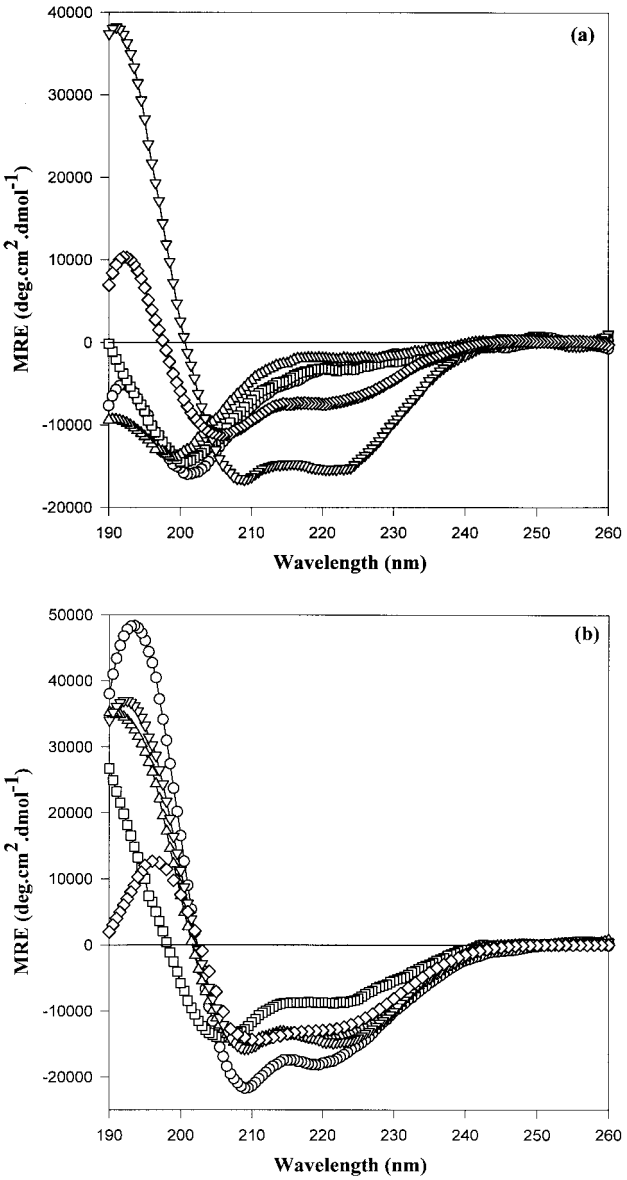


FIGURE 2: Far-UV CD spectra of 33mer peptides of apo A-I in PBS (a) and in 0.4% lysoPC micelles (b). Peptide concentration was ~100 $\mu$M. All the spectra were recorded at 25 °C using 0.01 cm cell on AVIV 62DS spectropolarimeter. Four scans were collected, averaged, and smoothed using the software provided by AVIV. Peptide G* (○), peptide 2−3 (□), peptide 3−4 (◇), peptide 8−9 (△), and peptide 9−10 (▽).

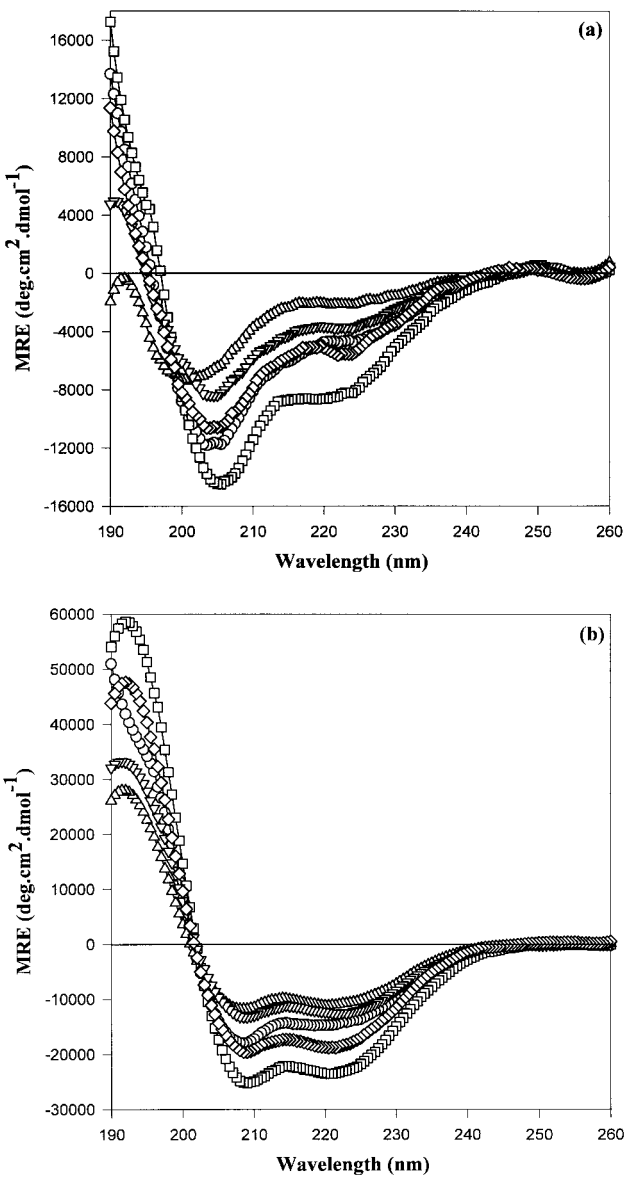


FIGURE 3: Far-UV CD spectra of 44mer peptides of apo A-I in PBS (a) and in 0.4% lysoPC micelles (b). Experimental conditions are same as described in Figure 2. Peptide 1−2 (○), peptide 4−5 (□), peptide 5−6 (△), peptide 6−7 (▽), peptide 7−8 (◇).

In PBS, the CD spectra of 33mer peptides, except for peptides 3−4 and 9−10, were consistent with a predominantly random structure (*29*) (Figure 2a). From the mean residue ellipticity at 222 nm (*32*), the helical contents of peptides 3−4 and 9−10 were estimated to be 26 and 47%, respectively. In 0.4% PPC micelles, CD spectra of all the 33mers were indicative of a helical structure (Figure 2b). It is interesting to note that the helical content of peptide 9−10 was similar in PBS and in PPC micelles (47 and 46%, respectively). Among 33mers, in PPC micelles the helical content of peptide G* was maximum (52%), while the helical content of peptide 2−3 was minimum (30%) (Figure 2b, Table 2).

In PBS, in contrast to 33mers, the CD spectra of 44mers, as evidenced by the presence of double minima at 208 and 222 nm, were indicative of helical structure (Figure 3a). The helical contents of the 44mers in PBS varied from 13% (peptide 5−6) to 29% (peptide 4−5) (Table 3). Similar to the 33mers, CD spectra of the 44mers in the PPC micelles indicated an increase in their helical contents (Figure 3b). Among the 44mers, in PPC micelles, peptides 4−5 and 5−6 exhibited the maximum (67%) and minimum (36%) helical contents, respectively (Figure 3b, Table 3).

The CD spectra of the 55mer, peptide 2−3−4, indicated 32 and 62% helicity in PBS and in the presence of PPC micelles, respectively (CD spectra not shown). The helical content of apo A-I is estimated to be 67, 81, and 93%, in PBS, in the presence of DMPC (lipid-to-protein ratio, 200: 1, M/M), and in PPC micelles (0.4%), respectively (CD spectra not shown). The helical contents of 33mer, 44mer, and 55mer peptides in 0.4% PPC micelles are summarized in Tables 2, 3, and 4, respectively.

As mentioned above, CD spectra of only five peptides could be recorded in the presence of DMPC (Figure 4). The CD spectra of all these five peptides are indicative of helical

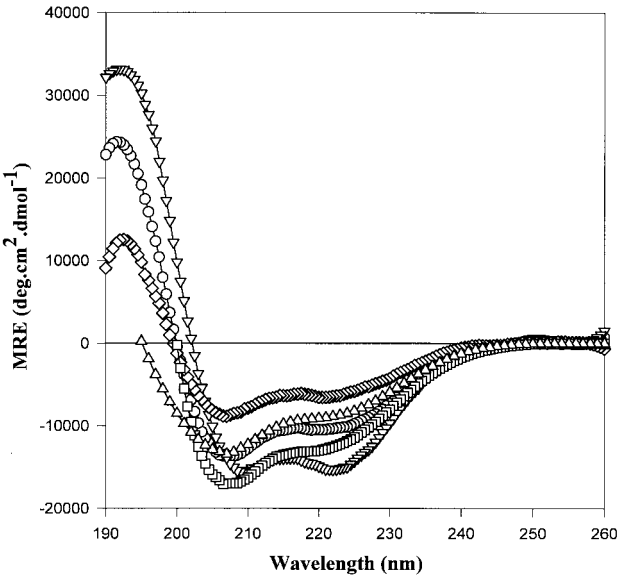


FIGURE 4: Far-UV CD spectra of 33mer, 44mer, and 55mer peptides of apo A-I in the presence of DMPC (lipid to peptide molar ratio 20:1). Other experimental conditions are same as described in Figure 2. Peptide G* (□), peptide 3−4 (◇), peptide 9−10 (▽), peptide 1−2 (○), peptide 2−3−4 (△).

Table 2: Comparison of the Properties of 33mer (and 22mer)[a] Synthetic Peptides of Human Apo A-I

| peptide | % helicity[b] | transition enthalpy ($\Delta H_T$, kcal/mol)[c] | exclusion pressure ($\pi_e$, dyn/cm)[d] | free energy of lipid association ($-\Delta G$, kcal/mol)[e] |
|---|---|---|---|---|
| peptide G* | 52 | 4.3 | 27 | 4.93 |
| peptide 2-3 | 30 | 7.0 | 20 | 3.98 |
| (peptide 2) | (22) | (5.6) | (17) | (3.50) |
| peptide 3-4 | 40 | 6.4 | 23 | 4.39 |
| (peptide 4) | (48) | (6.4) | (20) | (4.16) |
| peptide 8-9 | 44 | 6.4 | 27 | 4.39 |
| (peptide 8) | (36) | (6.3) | (23) | (3.39) |
| peptide 9-10 | 46 | 3.2 | 36 | 5.82 |
| (peptide 10) | (54) | (3.8) | (28) | (5.46) |

[a] Values taken from ref *16*. [b] In 0.4% PPC micelles. In PBS, helical contents of the peptides were peptide 3-4 (26%), peptide 4 (38%), peptide 9-10 (47%), and peptide 10 (26%). CD spectra of other peptides in PBS indicated random structure. [c] Enthalpy of the gel to liquid crystalline phase transition. The transition enthalpy for DMPC MLV alone is 7.0 kcal/mol. [d] Standard error in these measurements are ±1 dyn/cm. [e] Standard error in these estimates are ±0.1 kcal/mol.

conformation. Among the 33mers, peptide G* exhibited the maximum (53%), while peptide 3−4 exhibited the minimum (24%) helicity. It is interesting to note that peptide G*, which is random in buffer, adopts helical conformation in the presence of lipid. The helicity of peptide 9−10 was estimated to be 47%. The helical contents of peptides 1−2 and 2−3−4 were estimated to be 34 and 30%, respectively.

*Right-Angle Light-Scattering Measurements.* Exchangeable apolipoproteins as well as their synthetic amphipathic helical peptides possess the ability to transform DMPC MLV into protein−lipid (*38, 39*) or peptide−lipid (*21, 16*) discoidal complexes, respectively. The interaction of the peptides with MLV of DMPC was studied by monitoring the rate of clarification of the turbidity due to the lipid vesicles after the addition of the peptide. The results of this study are shown in Figure 5. Interaction of human apo A-I with MLV of DMPC is included for comparison. Among the 33mers, peptide 9−10 was most effective in solubilizing the MLV of DMPC (Figure 5a). The peptide G* was able to partially

Table 3: Comparison of the Properties of 44mer (and 22mer)[a] Synthetic Peptides of Human Apo A-I

| peptide | % helicity[b] | transition enthalpy ($\Delta H_T$, kcal/mol)[c] | exclusion pressure ($\pi_e$, dyn/cm)[d] | free energy of lipid association ($-\Delta G$, kcal/mol)[e] |
|---|---|---|---|---|
| peptide 1-2 | 45 | 4.6 | 31 | 5.40 |
| (peptide 1) | (45) | (4.8) | (30) | (4.51) |
| (peptide 2) | (22) | (5.6) | (17) | (3.50) |
| peptide 4-5 | 67 | 5.3 | 26 | 4.04 |
| (peptide 4) | (48) | (6.4) | (20) | (4.16) |
| (peptide 5) | (56) | (6.8) | (19) | (3.27) |
| peptide 5-6 | 36 | 7.0 | 27 | 2.79 |
| (peptide 5) | (56) | (6.8) | (19) | (3.27) |
| (peptide 6) | (54) | (6.8) | (19) | (3.92) |
| peptide 6-7 | 40 | 7.1 | 26 | 4.69 |
| (peptide 6) | (54) | (6.8) | (19) | (3.92) |
| (peptide 7) | (42) | (6.7) | (19) | (3.92) |
| peptide 7-8 | 55 | 6.7 | 29 | 4.63 |
| (peptide 7) | (42) | (6.7) | (19) | (3.92) |
| (peptide 8) | (36) | (6.3) | (23) | (3.39) |

[a] Values taken from ref *16*. [b] In 0.4% PPC micelles. In PBS, the helical contents of the peptides were peptide 1-2 (20%), peptide 4 (38%), peptide 4-5 (29%), peptide 5-6 (13%), peptide 6-7 (17%), peptide 7-8 (22%). CD spectra of other 22mers in PBS were indicative of random structure. [c] Enthalpy of the gel to liquid crystalline phase transition. The transition enthalpy for DMPC MLV alone is 7.0 kcal/mol. [d] Standard error in these measurements are ±1 dyn/cm. [e] Standard error in these estimates are ±0.1 kcal/mol.

solubilize the lipid vesicles (Figure 5a). Following an initial decrease, an increase in the light scattering was observed with peptide G*(Figure 5a). The reason for this is not clear at present. Other 33mer peptides did not solubilize MLV of DMPC (data not shown). Among the 44mer peptides, peptide 1−2 was most effective in the solubilization of MLV of DMPC (Figure 5b). Other 44mer peptides were not effective in solubilizing MLV of DMPC (data not shown). The peptide 2−3−4 did not clarify the turbidity due to MLV of DMPC in 30 min (data not shown). However, when the mixture was left overnight at room temperature, an optically clear solution of the peptide−lipid complex was obtained. It is interesting to note that apo A-I exhibited a slower rate of association with MLV of DMPC compared to the 33mer and 44mer peptides which were able to solubilize MLV of DMPC (Figure 5). The time required for a 50% decrease in the initial turbidity ($t_{1/2}$) for the peptides G*, 1−2, 9−10, and apo A-I were estimated to be ∼150, ≥30 ≤60, <30, and ∼360 s, respectively. The observed slower rate of apo A-I association presumably reflects a structural rearrangement required for apo A-I molecule(s) to associate with the DMPC vesicles.

*Electron Microscopy.* The peptide−DMPC and apo A-I−DMPC (lipid to peptide and lipid-to-protein ratio 2:1, w/w) mixtures were subjected to transmission electron microscopy to determine morphology and size of the resulting complexes. All the peptides which solubilized MLV of DMPC (Figure 5) formed discoidal peptide−lipid complexes. The electron micrographs are shown in Figure 6. While the peptides G* (15.6 ± 2.5 nm), 1−2 (16.4 ± 2.0 nm), and 9−10 (14.6 ± 2.8 nm) formed similar-sized discoidal complexes, peptide 2−3−4 formed larger (28.0 ± 4.0 nm) particles. Compared to the peptides, human apo A-I formed the smallest discoidal particles (9.6 ± 1.4 nm).

*Differential Scanning Calorimetry.* The effect of the peptides on the thermotropic phase transition properties of MLV of DMPC at a lipid to peptide molar ratio of 20:1 was

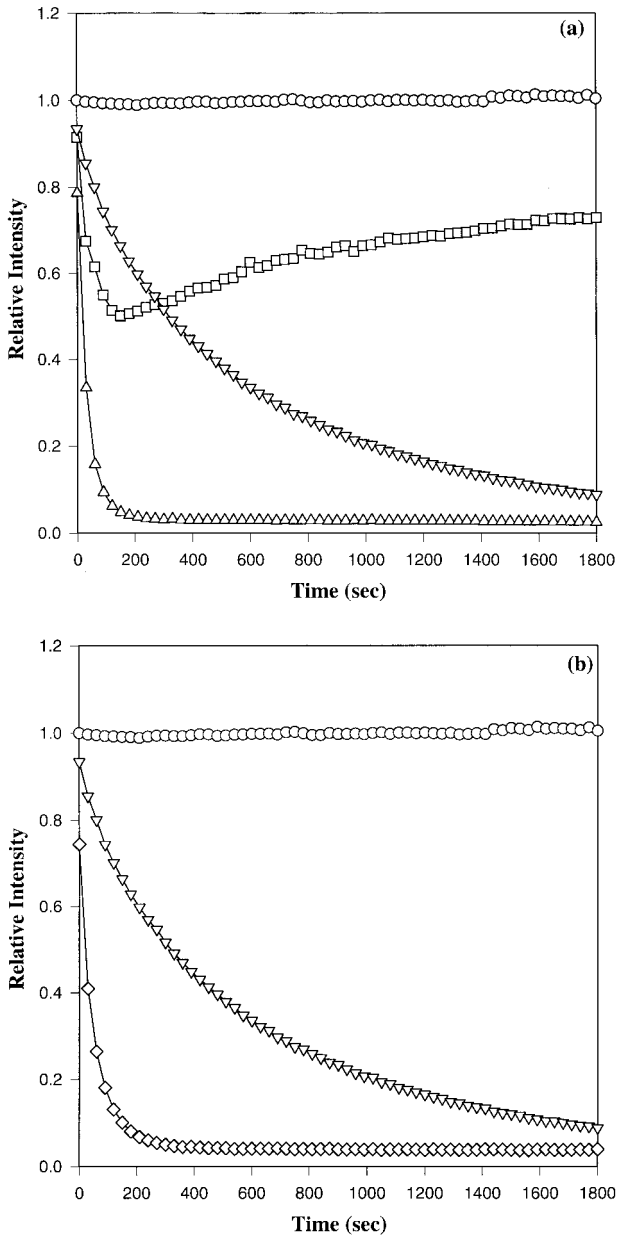


FIGURE 5: Relative decrease in scattered light intensity from DMPC MLVs after the addition of 33mer (a) and 44mer (b) peptides of apo A-I. Peptides were added to the vesicles at a 1:1 (w/w) ratio. All the measurements were carried out at 25 °C with constant magnetic stirring of the mixture using a SLM 8100 spectrofluorometer. Excitation and emission monochromators were both set at 400 nm and the band-passes were 4 nm each. The scattered light was detected at 90° from the incident beam and the data are presented relative to DMPC MLVs. (a) DMPC (○), peptide G* (□), peptide 9-10 (△), apo A-I (▽). Other 33mer peptides were not effective in solubilizing DMPC MLVs (data not shown). (b) DMPC (○), peptide 1−2 (◇), apo A-I (▽). Other 44mer peptides were not effective in solubilizing DMPC MLVs (data not shown).

investigated by high-sensitivity DSC. The heating endotherms of the MLV of DMPC in the absence and presence of the peptides are shown in Figure 7. In the absence of peptide, MLV of DMPC shows a pretransition at 13.0 °C and a gel to liquid−crystalline phase transition at 23.3 °C (Figure 7). The enthalpy ($\Delta H_T$) of the gel to liquid−crystalline phase transition of MLV of DMPC, measured as the total area under the peak, was estimated to be 7.0 kcal/mol. Association of the amphipathic helical peptides with MLV of DMPC often results in the lowering of the transition enthalpy as well as broadening of the transition because of the disruption of the highly ordered lipid bilayer structure (*40*−*43*, *16*). Among the 33mers, peptides G* and 9−10 caused significant reduction in the enthalpy of gel to liquid−crystalline phase transition of DMPC MLV; the peptide 9−10 ($\Delta H_T = 3.2$ kcal/mol) was more effective than peptide G* ($\Delta H_T = 4.3$ kcal/mol) in reducing the transition enthalpy (Table 2).

It is notable that apo A-I, at a lipid-to-protein ratio of 200:1 (M/M), reduces the enthalpy of the gel to liquid−crystalline phase transition of MLV of DMPC to the same extent [$\Delta H_T = 3.2$ kcal/mol (*16*)] as peptide 9−10, the most effective peptide, at a lipid-to-peptide ratio of 20:1 (M/M).

Although the transition enthalpy was not very much reduced in the case of peptide 3−4 ($\Delta H_T = 6.4$ kcal/mol), there was a noticeable broadening and splitting of the transition peak (Figure 7A and Table 2). The reason for the peak splitting is not clear at present. A noteworthy feature of the endotherm with the peptide G* is the presence of two distinctly separated chain melting peaks (Figure 7A, inset b). The temperature of the first peak corresponds to the chain melting temperature of DMPC vesicles in the absence of the peptide ($T_m = 23.3$ °C), whereas the temperature of the second peak is significantly higher ($T_m = 25.4$ °C) (Figure 7A, inset b). In the case of peptide 9−10, there is only one peak corresponding to the higher melting temperature ($T_m = 25.4$ °C) (Figure 7A, inset b). The presence of two distinct chain melting peaks in the endotherm with peptide G* could be because of the following two reasons: (i) incomplete solubilization of the DMPC MLV (this is consistent with the results of light scattering experiment, Figure 5a) and (ii) presence of peptide-poor and peptide-rich lipid domains in the resulting peptide−lipid complex. The peptide-rich lipid domain is expected to have chain melting transition occurring at higher temperature compared to the peptide-poor lipid domain, because of the restricted melting of the lipid acyl chains associated with the peptide molecules in the former case. Although we favor the first possibility, in the absence of other data at this stage, we cannot rule out the second possibility.

Among the 44mers, peptide 1−2 was the most effective in reducing the enthalpy of the gel to liquid−crystalline phase transition of MLV of DMPC ($\Delta H_T = 4.6$ kcal/mol) (Figure 7B, inset b, and Table 3). The peptide 4−5 reduced the transition enthalpy to a lesser extent ($\Delta H_T = 5.3$ kcal/mol). (Figure 7B, inset b, and Table 3). Significant broadening and splitting of the transition peak was observed in the case of peptide 7−8 (Figure 7B), similar to that observed for peptide 3−4 (Figure 7B), although the transition enthalpy was not greatly reduced ($\Delta H_T = 6.7$ kcal/mol) (Table 3). It is interesting to note that the endotherms with peptides 1−2 and 4−5 (Figure 7B, inset b) are also qualitatively similar to the endotherms with peptides 9−10 and G* (Figure 7A, inset b), respectively. The transition enthalpy, however, is lower with peptide 9−10 compared to peptide 1−2 (Table 3).

The heating endotherms of the MLV of DMPC in the presence of two 11mers, 3 and 9, and the 55mer, peptide 2−3−4, are shown in Figure 7C. The two 11mers did not affect the transition properties of the DMPC vesicles to a noticeable extent ($\Delta H_T = 7.1$ and 6.8 kcal/mol, for 3 and 9, respectively). However, peptide 2−3−4, reduced the en-

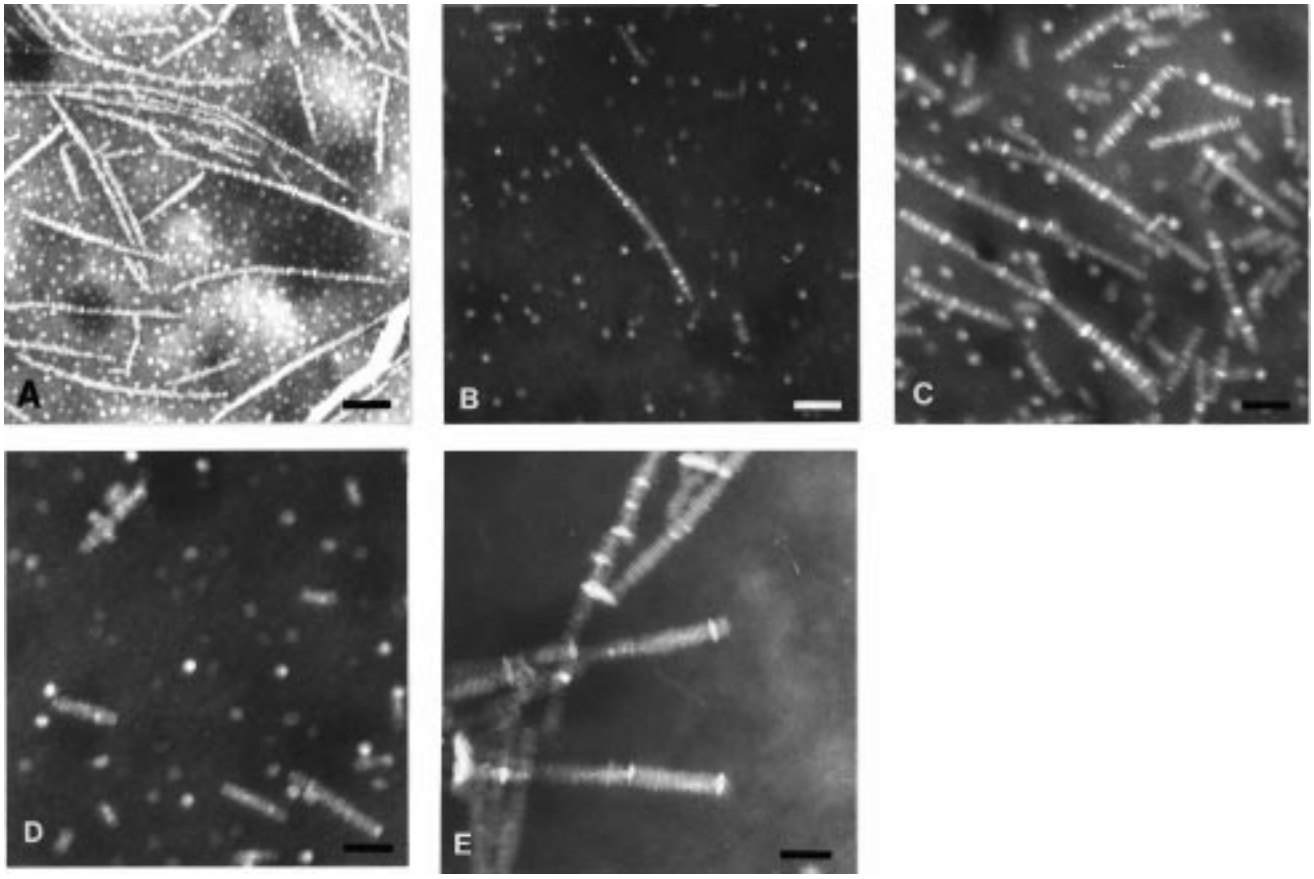


FIGURE 6: Electron micrographs of the discoidal DMPC complexes of apo A-I and peptides. (a) Apo A-I, (b) peptide 9−10, (c) peptide 1−2, (d) peptide G*, (e) peptide 2−3−4. Electron micrographs were taken at an instrument magnification of 50000× and an accelerating voltage of 75 kV. Bars indicate 100 nm.

thalpy of the gel to liquid−crystalline phase transition to a significant extent ($\Delta H_T = 4.5$ kcal/mol) (Figure 7C, inset b, and Table 4) and exhibited an endotherm qualitatively similar to the endotherms observed in the presence of peptides G* and 4−5 (Figure 7, panels A and 7B, insets b).

*Monolayer Exclusion Pressure Measurements.* The relative abilities of the peptides to penetrate an EYPC monolayer were determined by estimating their exclusion pressures. Among the 33mers, peptide 9−10 exhibited the highest exclusion pressure (36 dyn/cm), which is even higher than that of apo A-I (34 dyn/cm). The exclusion pressures for other 33mers are summarized in Table 2. Among the 44mers, peptide 1−2 exhibited the highest exclusion pressure (31 dyn/cm). The exclusion pressures for the other 44mers are summarized in Table 3. The exclusion pressures for the two 11mers, 3 and 9, were 12 and 15 dyn/cm, respectively. The exclusion pressure for the 55mer, peptide 2−3−4, was estimated to be 24 dyn/cm (Table 4).

*Partitioning of the Peptides into POPC MLV.* The free energy of lipid association ($\Delta G$) was estimated by measuring partitioning of the peptides into the MLV of POPC. Among the 33mers, peptide 9−10 exhibited the highest free energy of lipid association ($\Delta G = -5.82$ kcal/mol). The free energies of lipid association of all the 33mers are given in Table 2. Among the 44mers, peptide 1−2 exhibited the highest free energy of lipid association ($\Delta G = -5.40$ kcal/mol; Table 3). Consistent with the results of other experiments mentioned above, the free energy of lipid association of peptide 1−2 (Table 3) was lower than that of peptide 9−10 (Table 2). The free energy of lipid association of the 55mer, peptide 2−3−4, was estimated to be −4.39 kcal/mol (Table 4). Since the two 11mers, 3 and 9, did not show significant lipid affinity, either by DSC or by surface pressure measurements, their free energies of lipid association were not measured. The free energy of lipid association of apo A-I was estimated to be −4.83 kcal/mol, in close agreement with the value reported earlier (*33*).

## DISCUSSION

To evaluate the hypothesis that cooperativity among the adjacent amphipathic helical domains plays a major role in the lipid association of apo A-I, we have studied lipid-associating properties of 33mers, 44mers, and a 55mer peptide of apo A-I containing tandem amphipathic helical domains of apo A-I. The lipid-associating properties of these peptides have been compared with the lipid-associating properties of the 22mer peptides studied by us previously (*16*). This is the first study in which the postulated cooperativity among the adjacent amphipathic helical domains in the entire apo A-I sequence has been investigated.

*Experimentally Determined Lipid Affinities of Apo A-I Peptides.* CD spectra of all the peptides studied, except peptide 9−10, indicated an increase in their helical content in PPC micelles and in the presence of DMPC compared to that in PBS, indicating that they associate with phospholipids. The ability of peptide 9−10 to associate with phospholipids is established by other techniques, as discussed below.

A comparison of the helical contents of the peptides in DMPC versus that in PPC micelles reveals striking differ-

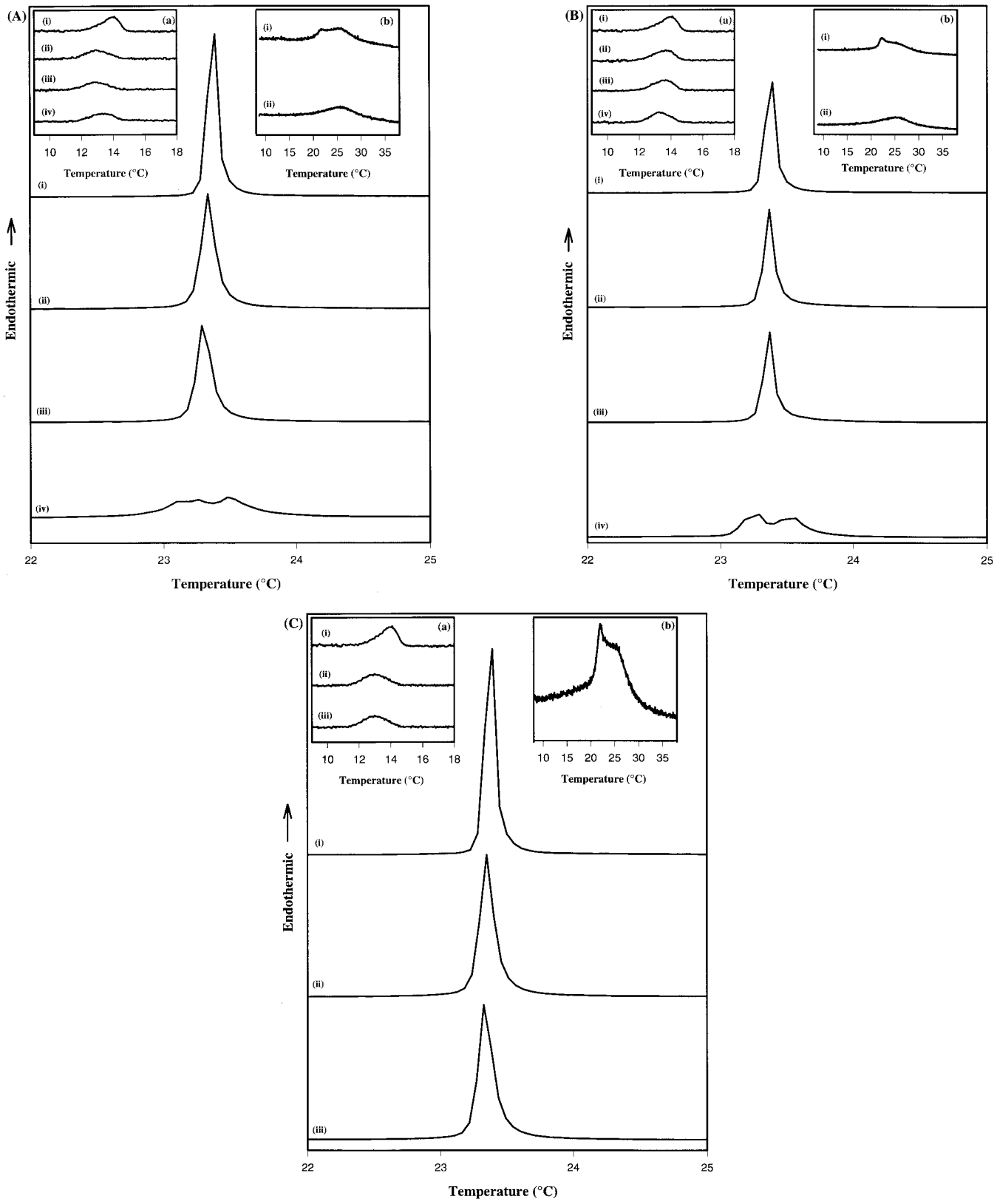


FIGURE 7: DSC heating endotherms of DMPC MLVs and mixtures of 33mer (A), 44mer (B) and 11mer and 55mer (C) peptides of apo A-I with DMPC MLVs. For the sake of clarity, the zero point on the *y*-axis has been arbitrarily adjusted for the heating endotherms. The heating endotherms presented as insets are enlarged to illustrate the fine structures of the thermograms. (A) DMPC (i), DMPC + peptide 2−3 (ii), DMPC + peptide 8−9 (iii), DMPC + peptide 3−4 (iv). Inset a shows the pretransition regions of the above samples enlarged. (Inset b): DMPC + peptide G* (i), DMPC + peptide 9−10 (ii); (B) DMPC (i), DMPC + peptide 6−7 (ii), DMPC + peptide 5−6 (iii), DMPC + peptide 7−8 (iv). Inset a shows the pretransition regions of the above samples enlarged. (Inset b): DMPC + peptide 4−5 (i), DMPC + peptide 1−2 (ii); (C) DMPC (i), DMPC + peptide 3 (ii), DMPC + peptide 9 (iii). Inset a shows the pretransition regions of the above samples enlarged. Inset b shows DMPC + peptide 2−3−4.

Table 4: Comparison of the Properties of 55mer (and 22mer)[a] Synthetic Peptides of Human Apo A-I

| peptide | % helicity[b] | transition enthalpy ($\Delta H_T$, kcal/mol)[c] | exclusion pressure ($\pi_e$, dyn/cm)[d] | free energy of lipid association ($-\Delta G$, kcal/mol)[e] |
|---|---|---|---|---|
| peptide 2-3-4 | 62 | 4.5 | 24 | 4.39 |
| (peptide 2) | (22) | (5.6) | (17) | (3.50) |
| (peptide 4) | (48) | (6.4) | (20) | (4.16) |

[a] Values are taken from ref *16*. [b] In 0.4% PPC micelles. In PBS, helical contents of peptide 2-3-4 and peptide 4 are 32% and 38%, respectively. CD spectra of peptides 2 and 3 in PBS were indicative of a predominantly random structure. [c] Enthalpy of the gel to liquid crystalline phase transition. The transition enthalpy for DMPC MLV alone is 7.0 kcal/mol. [d] Standard error in these measurements are ±1 dyn/cm. [e] Standard error in these estimates are ±0.1 kcal/mol.

ences in some cases. For example, while peptide 3−4 has 40% helicity in PPC, its helical content reduces to 24% in DMPC, which is similar to its helicity in PBS (26%). Similarly, the helical content of peptide 1−2 reduces from 45% in PPC micelles to 34% in DMPC. The helical content of the 55mer, peptide 2−3−4, also reduced from 62% in PPC micelles to 30% in the presence of DMPC, which is similar to its helicity in PBS (32%). The helical contents of peptides G* (52% in PPC versus 53% in DMPC) and 9−10 (46% in PPC versus 47% in DMPC) were similar in the two lipid environments. The environment is known to have a profound effect on the secondary structure adopted by the peptides (*44*, *45*). The higher helical contents in the presence of PPC micelles are presumably because of stronger interactions of the amphipathic peptides with PPC micelles compared to DMPC vesicles.

Results of the light-scattering experiments reveal that peptide 9−10 among the 33mers and peptide 1−2 among the 44mers are the most potent detergents. The rate of turbidity clarification was faster with peptide 9−10 compared to peptide 1−2. It is interesting to note that faster kinetics of peptide 9−10 is correlated with its higher helical content in PBS, which remains unchanged in PPC micelles and in the presence of DMPC. The peptides which showed a significant decrease in their helical contents in the presence of DMPC compared with that in PPC micelles, peptides 3−4 and 2−3−4, were not effective as detergents. While peptide 2−3−4 eventually solubilized DMPC vesicles (overnight incubation at room temperature), peptide 3−4 failed to do so. The slower rate of association of apo A-I with DMPC vesicles indicates that the molecule must undergo a structural change to associate with the lipid.

The solubilization of DMPC vesicles by the peptides was due to the formation of discoidal peptide−lipid complexes as revealed by EM studies (Figure 6). Among the peptides which formed discoidal complexes, peptide 2−3−4 formed the largest discoidal particles. It is interesting to note that human apo A-I formed discoidal particles which are even smaller than those formed by peptide 9−10, the peptide with highest lipid affinity (Figure 6). These results indicate that while apo A-I is able to stabilize smaller discoidal protein−lipid complexes that possess higher radius of curvature, the isolated peptides are not. Also, since peptide G* (a 33mer) and peptide 1−2 (a 44mer) form discoidal particles of similar size (particles formed by peptide 1−2 are slightly larger), there is no preferential stabilization of smaller discoidal particles due to the length of the peptide alone. This conclusion is further supported by our earlier observation that an 18 residue model peptide (18A) forms discoidal complexes with DMPC which are similar in size to those formed by apo A-I (*46*).

The results of DSC experiments correlate very well with the detergent property and the ability of the peptides to form discoidal complexes. The peptide 9−10 which showed the fastest kinetics of association with DMPC MLV and which formed the smallest discoidal particles caused the maximum reduction in the enthalpy of gel to liquid−crystalline phase transition of DMPC MLV. Apo A-I reduces the enthalpy of gel to liquid−crystalline phase transition of DMPC MLV to the same extent at a lipid-to-protein ratio of 200:1 (M/M) as the most effective peptide, peptide 9−10, at a lipid-to-peptide ratio of 20:1 (M/M). This indicates that all of the helical domains in apo A-I contribute in lipid association.

EYPC monolayer exclusion pressure measurements indicate that peptide 9−10 among the 33mers (Table 2) and peptide 1−2 among the 44mers (Table 3) possess the strongest ability to penetrate the monolayer. Among the 33mers and 44mers, peptides 9−10 and 1−2, respectively, also exhibit the highest free energy of lipid association (Tables 2 and 3). In contarst, an examination of the Tables 2, 3, and 4 reveals that the ability of the other peptides to penetrate an EYPC monolayer and their free energies of lipid association are not highly correlated. This presumably reflects differential abilities of the peptides to interact with phospholipid monolayer and multilamellar vesicles.

The role of amino acid residues 1−43 encoded by exon 3 of the apo A-I gene in the structure and function of apo A-I is not clear. A deletion mutant of apo A-I lacking this region [apo (Δ1−43) A-I] has been shown to possess lipid-associating properties similar to that of the intact apo A-I (*33*). This region contains the only class G* helix present in apo A-I (*23*). We have suggested previosly that class G* helixes can interact with either lipids or proteins depending upon the local environment (*5*). It is interesting to note that the peptide G* from this region has moderate lipid affinity. To our knowledge, this is the first study in which lipid-associating properties of the class G* helix present in apo A-I have been studied in detail.

*Is There Cooperativity among Adjacent Amphipathic α-helixes in apo A-I peptides for lipid-association?* The apo A-I sequence is composed of class G*, class $A_1$, and class Y amphipathic helixes [see Figure 1; (*23*)]. The apo A-I domains studied in the present work contain a combination of different classes of amphipathic helixes. The peptides studied and the class of amphipathic helix they belong to are as follows: peptide G* (G*), peptide 1−2 ($A_1 + A_1$), peptide 2−3 ($A_1 + Y$), peptide 3−4 ($Y + Y$), peptide 2−3−4 ($A_1 + Y + Y$), peptide 4−5 ($Y + A_1$), peptide 5−6 ($A_1 + A_1$), peptide 6−7 ($A_1 + A_1$), peptide 7−8 ($A_1 + A_1$), peptide 8−9 ($A_1 + Y$), and peptide 9−10 ($Y + Y$). We have shown recently using model amphipathic helical peptides that the class Y helix has higher lipid affinity than the class $A_1$ helix (*47*). Thus, a combination of $Y + Y$ helixes is expected to have higher lipid affinity than a combination of $A_1 + A_1$ helixes. These combinations are expected to be further strengthened as a result of cooperativity among the individual helixes. If it is true, one should be able to experimentally observe a higher lipid affinity (equal to or more than the sum of the lipid affinities of the constituent

helixes) resulting from the cooperativity among the adjacent amphipathic helixes.

The experimentally determined lipid-associating properties of 33mer, 44mer, and 55mer apo A-I peptides are summarized in Tables 2, 3, and 4, respectively. The lipid-associating properties of individual 22mers (*16*) are also included for comparison.

From a careful examination of Tables 2, 3, and 4, the following conclusions can be drawn. (1) Among the 33mers, peptide 9−10 exhibits the highest lipid affinity (Table 2). Since the 11mer, peptide 9, does not possess significant lipid affinity, the lipid affinity of peptide 9−10 is more than its constituent helixes (Table 2). The lipid affinities of the other 33mers increase marginally compared to the 22mers (Table 2). (2) For the 44mers, except for peptide 1−2 which has the highest lipid affinity among the 44mers, there is a minimal increase in the lipid affinity compared to the constituent 22mers (Table 3). (3) The 55mer, peptide 2−3−4, shows a marginal improvement in the lipid affinity compared to its constituent helixes (Table 4).

In summary, the results of this study indicate that, compared to 22mers, 33mer, 44mer, and 55mer peptides do not show a significant improvement in their lipid-associating properties. Considering that among the eight tandem 22mers, only N-terminal and C-terminal 22mers exhibited high lipid affinity, the results of the present study indicate that there is minimal cooperativity among the adjacent amphipathic helixes in the apo A-I domains for lipid association. All of the studies presented here clearly indicate that (i) peptide 9−10 is the most effective part of the apo A-I molecule for lipid association and (ii) the amphipathic helical domains from the central region of apop A-I possess weaker lipid affinity. The peptide G* containing the only class G* helix in apo A-I has moderate lipid affinity.

*Implications for the Structure and Function of Apo A-I.* The proposed models of apo A-I structure in the discoidal HDL particles indicate antiparallel arrangement of tandem amphipathic helical domains separated by proline containing $\beta$-turns and stabilized by interhelix salt-bridge formation (*6*, *12*, *13*, *48*). However, a recent computer model of the dimeric apo A-I structure in the reconstituted HDL disks indicates protein−lipid interaction as the primary factor in stabilizing the complex and does not support strong interhelical interactions (*49*). Since this model does not include residues 1−47 of apo A-I, evaluation of *intramolecular* interhelical interactions between the N-terminal and C-terminal helixes has not been possible (*49*). It has been suggested that for the apo A-I dimer both head-to-head and head-to-tail arrangements are possible (*49*).

The structure of apo (Δ1−43) A-I has been determined recently using X-ray crystallography (*50*). The crystal structure supports a "belt model" of apo A-I in discoidal HDL particles (*50*), as opposed to the earlier "picket fence" model (reviewed in ref *6*). In the belt model, amphipathic helical domains of apo A-I are arranged perpendicular to the lipid acyl chains, whereas in the picket fence model, they are arranged parallel to the lipid acyl chains. Whereas, the picket fence model of apo A-I is supported by ATR-FTIR studies (*48*, *51*), no independent experimental evidence at the present time exists supporting the belt model. In the crystal structure (*50*), helixes 4, 5, and 6 form a bend, with helix 5 forming the center of the bend. It is interesting to note that among all of the amphipathic helical domains studied, helix 5 has the smallest free energy of lipid association (Table 3). In the crystal structure, the residues 220−227 adopt an extended, nonhelical conformation (*50*). This region possesses alternating polar and nonpolar amino acid residues. It is interesting to note that, compared to the other amphipathic helical domains, peptide 10 encompassing this region has the highest overall hydrophobicity (data not shown) and highest free energy of lipid association (Table 2).

From the above studies as well as our own studies with apo A-I reported in this paper, it is evident that in the discoidal HDL particles, the structure of apo A-I is stabilized by cooperative interactions. This cooperativity is minimal in the apo A-I fragments as shown by the studies of the synthetic peptides containing tandem multiple amphipathic helixes. It is likely that the structure of apo A-I in the discodal HDL particles is stabilized by both *intermolecular*, as suggested by the crystal structure of apo (Δ1−43) A-I (*50*), as well as *intramolecular* (e.g., interactions between N- and C-terminal end helixes) interhelical interactions.

The results of the present study clearly indicate that, compared to the N- and C-terminal amphipathic helical domains, the central amphipathic helical domains in apo A-I in general, and helix 5 in particular, have weaker lipid affinities (Table 3). It is interesting to note that the central amphipathic helical domains in apo A-I have been implicated in the LCAT activation (*52*). The weaker lipid affinity of the central amphipathic helical domains in apo A-I may be essential for the LCAT activation. This is supported by a recent study in which substitution of a strongly lipid-associating amphipathic helical domain (helix 10) for a weakly lipid-associating amphipathic helical domain in the central part of apo A-I (helix 6) results in a 5−6-fold decrease in the LCAT activation by the mutant protein compared to the wild-type apo A-I (*53*). It is likely that the central amphipathic helical domains in apo A-I with lower lipid affinities are involved in the interaction of the protein with the enzyme. Such protein−protein interactions involving the central amphipathic helical domains of apo A-I may also be important in the recognition of HDL particles by its receptor (*54*).

## ACKNOWLEDGMENT

We thank Dr. Donald D. Muccio, Chemistry Department, UAB, for the use of spectropolarimeter. We also thank Dr. Stephen Barnes and Mr. Marian Kirk of the mass spectrometry core facility and Mr. Eugene D. Arms of the electron microscopy core facility of the UAB Cancer Center for their help with the sample analyses.

## REFERENCES

1. Chajek-Shaus, T., Hayek, T., Walsh, A., and Breslow, J. L. (1991) *Proc. Natl. Acad. Sci. U.S.A. 88*, 6731−6735.
2. Rubin, E. M., Krauss, R. M., Spangler, E. A., Verstuyft, J. G., and Clift, S. M. (1991) *Nature 353*, 265−267.
3. Schulz, J. R., Verstuyft, J. G., Gong, E. L., McCall, M. R., Nichols, A. V., and Rubin, E. M. (1993) *Nature 365*, 762−764.
4. Warden, C., Hedrick, C. C., Quao, J.-H., Castillani, L. W., and Lusis, A. J. (1993) *Science 261*, 469−471.

5. Segrest, J. P., Garber, D. W., Brouillette, C. G., Harvey, S. C., and Anantharamaiah, G. M. (1994) *Adv. Protein Chem. 45*, 303−369.
6. Brouillette, C. G., and Anantharamaiah, G. M. (1995) *Biochim. Biophys. Acta 1256*, 103−129.
7. Jonas, A. (1991) *Biochim. Biophys. Acta 1084*, 205−220.
8. Johnson, W. J., Mahlberg, F. H., Rothblat, G. H., and Phillips, M. C. (1991) *Biochim. Biophys. Acta 1085*, 273−298.
9. Fielding, C. J., and Fielding, P. E. (1995) *J. Lipid Res. 36*, 211−228.
10. Oram, J. F., and Yokoyama, S. (1996) *J. Lipid Res. 37*, 2473−2491.
11. Collet, X., Perret, B., Simard, G., Raffai, E., and Marcel, Y. L. (1991) *J. Biol. Chem. 266*, 9145−9152.
12. Marcel, Y. L., Provost, P. R., Koa, H., Raffai, E., Dac, N. V., Fruchart, J. C., and Rassart, E. (1991) *J. Biol. Chem. 266*, 3644−3656.
13. Nolte, R. T., and Atkinson, D. (1992) *Biophys. J. 63*, 1221−1239.
14. Jonas, A., von Eckardstein, A., Churgay, L., Mantulin, W. W., and Assmann, G. (1993) *Biochim. Biophys. Acta 1166*, 202−210.
15. Sparks, D. L., Lund-Katz, L., and Phillips, M. C. (1992) *J. Biol. Chem. 267*, 25839−25847.
16. Palgunachari, M. N., Mishra, V. K., Lund-Katz, S., Phillips, M. C., Adeyeye, S. O., Alluri, S., Anantharamaiah, G. M., and Segrest, J. P. (1996) *Arteriscler. Thromb. Vasc. Biol. 16*, 328−338.
17. Sparrow, J. T., and Gotto, A. M., Jr. (1982) *CRC Crit. Rev. Biochem. 13*, 87−107.
18. Kroon, D. J., and Kaiser, E. T. (1978) *J. Org. Chem. 43*, 2107−2113.
19. Fukushima, D., Yokoyama, S., Kroon, D. J., Kézdy, F. J., and Kaiser, E. T. (1980*) J. Biol. Chem. 255*, 10651−10657.
20. Sparrow, J. T., and Gotto, A. M., Jr. (1980) *Ann. N. Y. Acad. Sci. 348*. 187−211.
21. Vanloo, B., Demoor, L., Boutillon, C., Lins, L., Brasseur, R., Baert, J., Fruchart, J. C., Tartar, A., and Rosseneu, M. (1995) *J. Lipid Res. 36*, 1686−1696.
22. Venkatachalapathi, Y. V., Phillips, M. C., Epand, R. M., Epand, R. F., Tytler, E. M., Segrest, J. P., and Anantharamaiah, G. M. (1993) *Proteins: Struct., Funct., Genet. 15*, 349−359.
23. Segrest, J. P., Jones, M. K., De Loof, H., Brouillette, C. G., Venkatachalapathi, Y. V., and Anantharamaiah, G. M (1992) *J. Lipid Res. 33*, 141−166.
24. Anantharamaiah, G. M., and Garber, D. W. (1996) *Methods Enzymol. 263*, 267−282.
25. Ebert, R. F. (1986) *Anal. Biochem. 154*, 431−435.
26. Ames, B. N. (1966) *Methods Enzymol. 8*, 115−118.
27. Yang, J. T., Wu, C.-S, C., and Martinez, H. M. (1986) *Methods Enzymol. 130*, 208−269.
28. Johnson, W. C., Jr. (1990) *Proteins: Struct., Funct., Genet. 7*, 205−214.
29. Woody, R. W. (1995) *Methods Enzymol. 246*, 34−71.
30. Jonas, A. (1986) *Methods Enzymol. 128*, 553−582.
31. Morrisett, J. D., David, J. S. K., Pownall, H. J., and Gotto, A. M., Jr. (1973) *Biochemistry 12*, 1290−1299.
32. Spuhler, P., Anantharamaiah, G. M., Segrest, J. P., and Seelig, J. (1994) *J. Biol. Chem. 269*, 23904−23910.
33. Rogers, D. P., Brouillette, C. G., Engler, J. A., Tendian, S. W., Roberts, L., Mishra, V. K., Anantharamaiah, G. M., Lund-Katz, S., Phillips, M. C., and Ray, M. J. (1997) *Biochemistry 36*, 288−300.
34. Phillips, M. C., and Krebs, K. E. (1986) *Methods Enzymol. 128*, 387−403.
35. Ibdah, J. A., Krebs, K. E., and Phillips, M. C. (1989) *Biochim. Biophys. Acta 1004*, 300−308.
36. Anantharamaiah, G. M., Hughes, T. A., Iqbal, M., Gawish, A., Neame, P. J., Meradley, M. F., and Segrest, J. P. (1988) *J. Lipid Res. 29*, 309−318.
37. Narayanaswami, V., Kay, C. M., Oikawa, K., and Ryan, R. O. (1994) *Biochemistry 33*, 13312−13320.
38. Surewicz, W. K., Epand, R. M., Pownall, H. J., and Hui, S. W. (1986) *J. Biol. Chem. 261*, 16191−16197.
39. Jonas, A., Kézdy, K. E., and Wald, J. H. (1989) *J. Biol. Chem. 264*, 4818−4824.
40. Morrisett, J. D., Jackson, R. L., and Gotto, A. M., Jr. (1977) *Biochim. Biophys. Acta 472*, 93−133.
41. McLean, L. R., Buck, S. H., and Krstenansky, J. L. (1990) *Biochemistry 29*, 2016−2022.
42. Mishra, V. K., Palgunachari, M. N., Segrest, J. P., and Anantharamaiah, G. M. (1994) *J. Biol. Chem. 269*, 7185−7191.
43. Mishra, V. K., Palgunachari, M. N., Lund-Katz, S., Phillips, M. C., Segrest, J. P., and Anantharamaiah, G. M. (1995) *J. Biol. Chem. 270*, 1602−1611.
44. Zhong, L. and Johnson, W. C., Jr. (1992) *Proc. Natl. Acad. Sci. U.S.A. 89*, 4462−4465.
45. Waterhous, D. V. and Johnson, W. C., Jr. (1994) *Biochemistry 33*, 2121−2128.
46. Anantharamaiah, G. M., Jones, J. L., Brouillette, C. G., Schmidt, C. F., Chung, B. H., Hughes, T. A., Bhown, A. S., and Segrest, J. P. (1985) *J. Biol. Chem. 260*, 10248−10255.
47. Mishra, V. K., and Palgunachari, M. N. (1996) *Biochemistry 35*, 11210−11220.
48. Brasseur, R., De Meutter, J., Vanloo, B., Goormaghtigh, E., Ruysschaert, J. M., and Rosseneu, M. (1990) *Biochim. Biophys. Acta 1043*, 245−252.
49. Phillips, J. C., Wriggers, W., Li, Z., Jonas, A., and Schulten, K. (1997) *Biophysical J. 73*, 2337−2346.
50. Borhani, D. W., Rogers, D. P., Engler, J. A., and Brouillette, C. G. (1997) *Proc. Natl. Acad. Sci. U.S.A. 94*, 12291−12296.
51. Wald, J. H., Goormaghtigh, E., Meutter, J. D., Ruysschaert, J.-M., and Jonas, A. (1990) *J. Biol. Chem. 265*, 20044−20050.
52. Sorci-Thomas, M. G., Kearns, M. W., and Lee, J. P. (1993) *J. Biol. Chem. 268*, 21403-21409.
53. Sorci-Thomas, M. G., Curtiss, L., Parks, J. S., Thomas, M. J., and Kearns, M. W. (1997) *J. Biol. Chem. 272*, 7278−7284.
54. Acton, S., Rigotti, A., Landschulz, K. T., Xu, S., Hobbs, H. H., and Krieger, M. (1996) *Science 271*, 518−520.
55. Anantharamaiah, G. M., Jones, M. K., and Segrest, J. P. (1993) in *The Amphipathic Helix* (Epand, R. M., Ed.) pp 109−142, CRC Press, Boca Raton, FL.


BI980042O